Coexistence of para and ferromagnetic phases of Fe^{3+} in undoped CdZnTe (Zn ~ 4%) crystals

Gururaj Anand Kulkarni [a,*], Oruganty V.S.N. Murthy [a], K.S.R.K. Rao [a], S.V. Bhat [a], B.R. Chakraborty [b]

[a] Department of Physics, Indian Institute of Science, Bangalore - 560012, India
[b] National Physical Laboratory, New Delhi - 110012, India

A B S T R A C T

The signatures of the coexistence of para and ferromagnetic phases for the Fe^{3+} charge state of iron have been identified in the low temperature electron spin resonance (ESR) spectra in undoped CdZnTe (Zn ~ 4%) crystals and independently verified by superconducting quantum interference device (SQUID) and AC susceptibility measurements. In the paramagnetic phase the inverse of AC susceptibility follows the Curie–Weiss law. In the ferromagnetic phase the thermal evolution of magnetization follows the well-known Bloch $T^{3/2}$ law. This is further supported by the appearance of hysteresis in the SQUID measurements at 2 K below T_C which is expected to lie in between 2 and 2.5 K.

1. Introduction

It is well known that $Cd_{0.96}Zn_{0.04}Te$ material remains the substrate of choice for the epitaxial growth of HgCdTe for use in high performance IR detectors and focal plane arrays [1]. Such applications require high quality and defect free $Cd_{0.96}Zn_{0.04}Te$ substrate material with high optical transmission. However, the as-grown CdZnTe crystals suffer from defects, impurities and second phase Te precipitates [2–5]. According to mass spectroscopic data, Fe could occur in CdTe crystals as an unintentional impurity in concentrations of up to 10^{17} cm^{-3} [6]. Moreover, the solubility of iron at the melting point of CdTe was in excess of 10^{20} cm^{-3} [7]. The results of annealing experiments carried out on CdTe at $T > 800$ °C have shown that this material could become contaminated with iron captured from insufficiently purified quartz [6]. Control of iron impurity in CdTe appears to be of great importance if the material is to be used as a substrate for epitaxial growth of $Hg_{1-x}Cd_xTe$, since out diffusion of iron from the substrate into the epilayer deleteriously affects the performance of $Hg_{1-x}Cd_xTe$ infrared detectors [8]. On the contrary the incorporation of Fe can lead to interesting magnetic properties in semiconductors for spintronic applications [9]. In this connection the coexistence of para and ferromagnetic phases reported in this letter, in the undoped CdZnTe crystals due to the unintentional incorporation of Fe^{3+} may be of interest for further investigations into the magnetic properties of intentionally Fe doped CdZnTe crystals, for the possible spintronic applications.

2. Experimental details

Undoped CdZnTe (Zn ~ 4%) crystals were grown by asymmetrical Bridgman method using evacuated, sealed carbon-coated GE-214 grade, OH content less than 5 ppm quartz tubes, in a three-zone furnace. Single crystal wafers having ⟨111⟩ orientation were cut from the grown ingots and used for sample preparation. The details of sample growth and preparation methods are same as depicted earlier [3,5]. An ultra-high vacuum quadruple ion microprobe, model MIQ 256 CAMECA–RIBER has been used for secondary ion mass spectrometry (SIMS) measurements [10]. The spectra were collected after sputter cleaning the top surface over an area of 200 μm^2 for 10 min using Ga^+ primary beam of 25 keV energy with beam current of 4 nA. ESR measurements were carried out using a Bruker spectrometer in the *X*-band with a microwave frequency of 9.43 GHz in the temperature range from 5 to 300 K. AC susceptibility measurements were performed using commercial CRYOBIND system down to a temperature of 4.2 K at a frequency of 420 Hz and an applied ac magnetic field of 178 mOe (~0.224 mT). The magnetization measurements were carried out in a SQUID magnetometer (Quantum Design). Low temperature

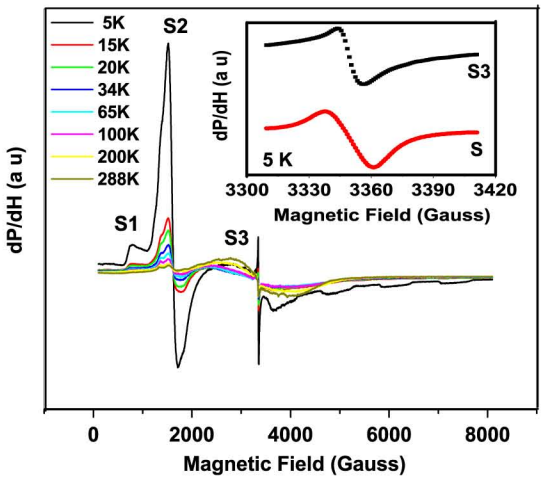

Fig. 1. (Color online or on the web only) Temperature dependent ESR spectra of undoped CdZnTe (Zn ~ 4%) crystal. Inset shows simulation (S) of signal $S3$ using $+5/2$ spin state of Fe^{3+}.

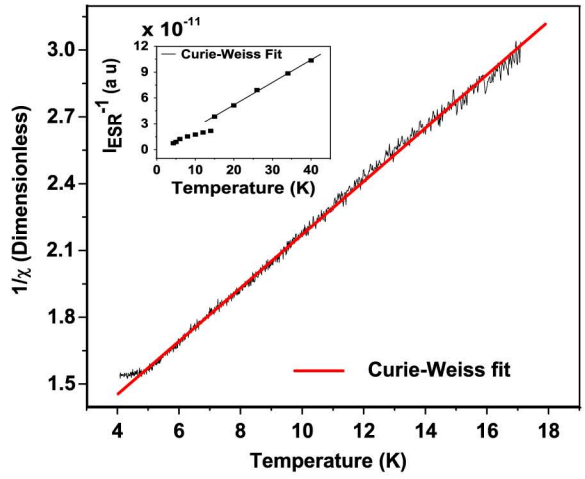

Fig. 2. (Color online or on the web only) The inverse of AC susceptibility versus temperature plot showing the Curie–Weiss behavior down to 4.8 K. The inverse of ESR intensity of signal $S2$ follows the Curie–Weiss behavior down to 15 K, as shown in the inset.

Fourier transform infrared (FTIR) absorption spectra were recorded over 400–4500 cm^{-1} (i.e. 0.04–0.45 μm) range using BRUKER's (IFS) 66 V/s spectrometer at a resolution of 4 cm^{-1} [5].

3. Results and discussion

To begin with SIMS measurements were carried out on a series of samples taken from different CdZnTe ingots. Only those samples which showed iron impurity were further subjected to magnetization measurements.

Fig. 1 shows the typical temperature dependent ESR spectra of such undoped CdZnTe (Zn ~ 4%) crystal. Three resonant signals can be identified from Fig. 1 marked around the central fields of 800 G (or 0.08 T) (for signal $S1$), 1616 G (or 0.1616 T) (for signal $S2$) and 3349 G (or 0.3349 T) (for signal $S3$) respectively at 5 K. These resonance signals are not angular dependent and their intensities do not vary significantly upon rotating the magnetic field from parallel to perpendicular with respect to ⟨111⟩ direction.

Signal $S3$ is the sharpest with the peak to peak line width of $\Delta H_{PP} = 13$ G (1.3 mT) at 5 K and has been analyzed using the $S = +5/2$ spin Hamiltonian (1) and simulated using the Easy Spin program;

$$H = g\mu_B BS + D[S_z^2 - S(S+1)/3] + E(S_x^2 - S_y^2), \quad (1)$$

where the first term accounts for the Electron Zeeman Interaction (EZI) and the second and third represent Zero-Field Interaction (ZFI) of the electron spin. All the parameters used have their usual meaning. Simulating with the experimentally observed line width at 5 K, an overall agreement in intensity was obtained for signal $S3$ as shown in the inset of Fig. 1 and the following best fit parameters were extracted. (1) An isotropic value of $g = 1.9689 \pm 0.0001$, (2) $D = 5946.38 \pm 0.01$ and $E = 1.5816 \times 10^{-6}$ MHz, the parameters of the fine structure tensor.

The isotropic g value obtained deviates strongly from the free electron g value of 2.0023 and exhibits a negative g shift. Positive g-shifts, however, have been reported on Fe^{3+} ion which replaces cations in cubic crystals, for instance, MgO, CaO and ZnS [11]. Fidone and Stevens [12] suggest that there will be a contribution to the g-shift from electron transfer processes through spin–orbit interaction from the ligands to the S-state ion or the reverse transfer, and that the former transfer leads to a positive and the latter to a negative g-shift. The idea of electron transfer was put in to a more detailed calculation for Fe^{3+} in the II–VI cubic crystals by Watanabe [11], to show that the g-shift calculated is favorably compared to the observed g-shifts of Fe^{3+} in MgO, CaO and ZnS. From the above discussions, following Fidone and Stevens [12] arguments, the observed negative g-shift may be attributed to the electron transfer processes through spin–orbit interaction from the Fe^{3+} ion to the surrounding Te ligands in the tetrahedral symmetry.

It has been found that most of the manganites show a coexistence of more than one phase. The presence of more than one ESR line has been attributed to secondary phases [13]. Fig. 1 also shows the temperature dependence of low field signal $S2$ with characteristic Dysonian line shape, may be due to skin depth effects, [14,15] leading to an analysis in this direction. For the accurate determination of various line shape parameters, the signals ($S2$) were fitted to the modified double Dysonian line shape function (2) consisting of clockwise and anticlockwise circularly polarized components of microwave radiation [16].

$$\frac{dP}{dH} = \frac{d}{dH}\left[\frac{\Delta H_{FWHM} + \alpha(H - H_o)}{4(H - H_o)^2 + \Delta H_{FWHM}^2} + \frac{\Delta H_{FWHM} - \alpha(H + H_o)}{4(H + H_o)^2 + \Delta H_{FWHM}^2}\right], \quad (2)$$

where H_o is the central field, ΔH_{FWHM} is the full width at half maximum and α is fraction of the dispersion component added into the absorption signal.

Inverse of AC susceptibility and inverse of ESR intensity for signal $S2$ follow the Curie–Weiss law down to 4.8 and 15 K, as shown in Fig. 2 and the inset respectively. ESR technique can detect Fe concentrations of less than 0.1 ppm in CdTe [17]. Hence for macroscopic magnetization Curie temperature $T_C < 4.8$ K may be considered as given by the change in slope to the inverse of AC susceptibility (Fig. 2). Also from the Curie–Weiss fit to the inverse of AC susceptibility the Curie constant $C = 8.36$ was determined. The effective paramagnetic moment was calculated to be 5.8241 in units of μ_B the Bohr magneton. For the accurate determination of T_C, Arrot plots (H/M versus M^2 isotherms) were made out of the SQUID magnetization data and are shown in Fig. 3. It is apparent from these plots that one of the isotherms between 2 and 2.5 K crosses the origin. Therefore the T_C is expected to lie in between 2 and 2.5 K.

The thermal evolution of magnetization in the ferromagnetic phase was fitted to the Bloch $T^{3/2}$ law

$$[M(0,0) - M(H,T)] = 2.612 g\mu_B [k_B T/4\pi D]^{3/2}, \quad (3)$$

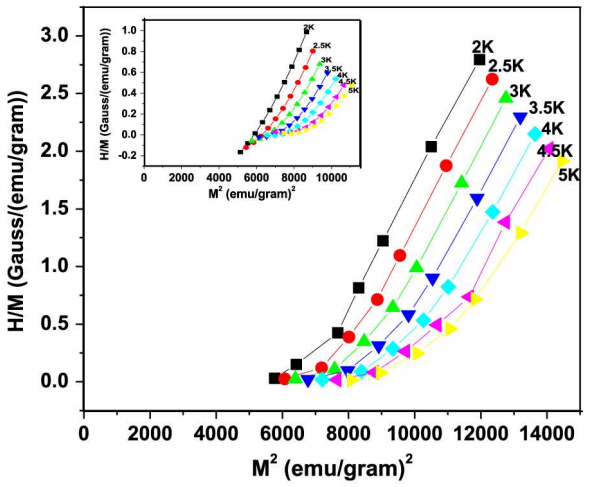

Fig. 3. (Color online or on the web only) Arrot plot for the determination of T_C. Inset is the expanded version of the second order polynomial fits to the H/M versus M^2 isotherms which depicts T_C to lie in between 2 and 2.5 K.

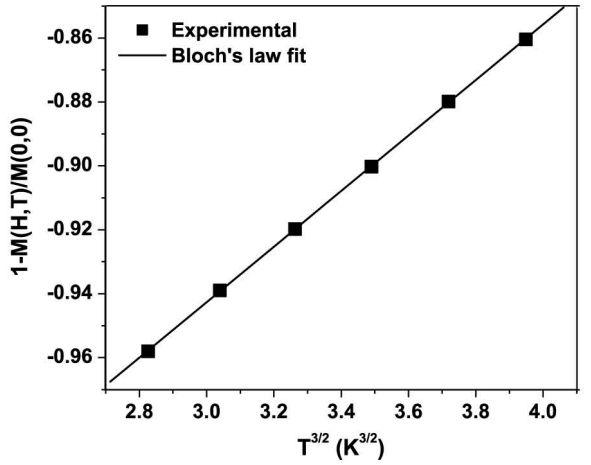

Fig. 4. Shows the Bloch $T^{3/2}$ law fit to the low temperature thermal evolution of magnetization.

as shown in Fig. 4 [18]. Here g is the g-factor and k_B is the Boltzmann constant. $M(0,0)$ was obtained by extrapolating $M(H,T)$ curves to $T = 0$ and $H = 0$ using a second order polynomial. From the slope of the linear fit to the data of $[1 - M(H,T)/M(0,0)]$ versus $T^{3/2}$ plot, the value of spin-stiffness constant $D = 3.9526 \pm 0.0001$ meVÅ^2 was determined. The value of spin-stiffness constant is a measure of the strength of coupling among the spins.

The appearance of hysteresis in the SQUID measurements at 2 K (Fig. 5) further confirms the ferromagnetic phase formation below T_C. Inset (a) in Fig. 5 is the expanded part of M–H curve near $H = 0$ at 2 K, with a small coercive field of 10 Oe (~0.013 T), which suggests that the magnetic anisotropy is very small in these systems. Inset (b) in Fig. 5 shows the M–H isotherm at 10 K and it clearly indicates that the nonlinear behavior of the M–H isotherm weakens fast on increasing the temperature above T_C.

Fig. 6 shows the FTIR transmission spectra of the undoped CdZnTe crystal at 3 K. The absorption at 2295 cm^{-1} (~0.23 μm) may be attributed to electron transition from ν_1 level of ^{5}E (10 fold degenerate) to Γ_4 level of $^5T_2$ (15 fold degenerate), when Fe^{2+} ion substitutes for Cd^{2+} in a site of tetrahedral symmetry T_d [19,20]. Strong absorption around 2650 cm^{-1} (~0.27 μm) corresponding to the band gap of tellurium (0.33 eV) indicates the presence of tellurium precipitates in the CdZnTe crystals [5].

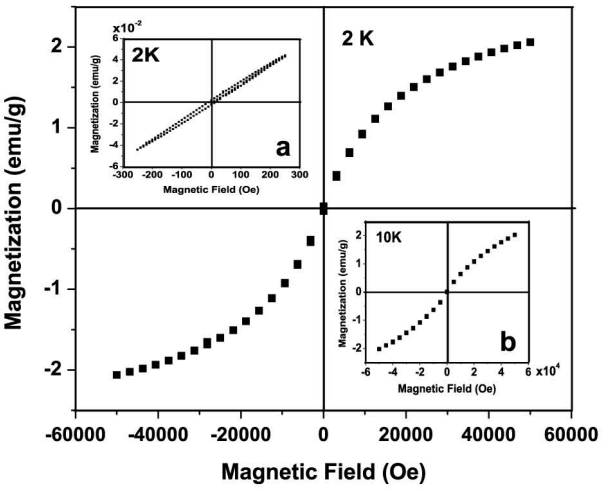

Fig. 5. Magnetization versus magnetic field (M–H) plot at 2 K for CdZnTe crystal. Inset (a) is the expanded part of M–H curve near $H = 0$ at 2 K, which shows a small hysteresis loop with a coercive field of 10 Oe (~ 0.013 T). Inset (b) shows the M–H isotherm at 10 K.

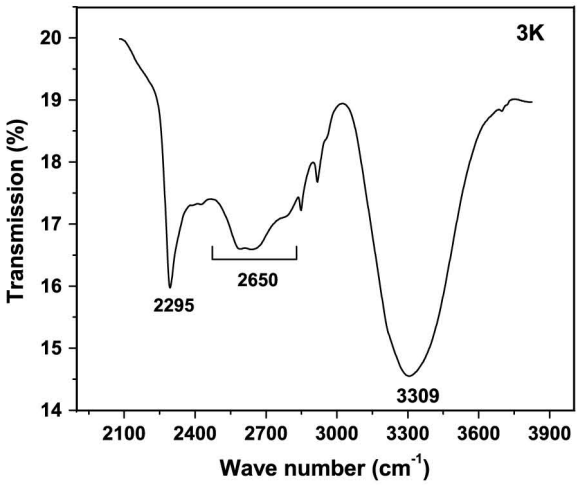

Fig. 6. Shows the FTIR transmission spectra of the undoped CdZnTe crystal at 3 K. The absorption at 2295 cm^{-1} (~0.23 μm) and 3309 cm^{-1} (~0.33 μm) may be attributed to Fe^{2+} ($3d^6$) impurity and cadmium vacancy defect respectively, in CdZnTe. Strong absorption around 2650 cm^{-1} (~0.27 μm) corresponding to the band gap of tellurium (0.33 eV) indicates the presence of tellurium precipitates in the CdZnTe crystal.

These Te precipitates may condense as Cd vacancies during the cooling process leading to cadmium vacancy point defects [4]. The absorption at 3309 cm^{-1} (~0.33 μm) may be attributed to cadmium vacancy point defects [21].

FTIR results clearly show that the presence of iron leads to loss of useful signal in the 2–6 μm infrared (IR) window and hence harmful for the substrate application of CdZnTe required for the growth and fabrication of HgCdTe IR detectors.

4. Conclusions

The presence of Fe as an unintentional impurity in undoped CdZnTe (Zn ~ 4%) crystals has been identified and characterized by various physical techniques and hence found to have Fe^{2+} and Fe^{3+} charge states. The doubly ionized charge state Fe^{2+} being optically active shows strong absorption around 2295 cm^{-1} in the low temperature FTIR spectra, while Fe^{3+} being magnetically active exhibits phase coexistence. In the paramagnetic phase the inverse of AC susceptibility follows Curie–Weiss law. In the ferromagnetic phase the thermal evolution of magnetization follows the well-known Bloch $T^{3/2}$ law. The appearance of hysteresis in the

SQUID measurements at 2 K further supports the transition to ferromagnetic phase below T_C which is shown to lie in between 2 and 2.5 K.

Acknowledgements

We acknowledge Ajay Sharma and S.S. Rao for ESR measurements. Also we acknowledge Prof. Anil Kumar for his permission to conduct the AC susceptibility measurements and Vishwanath for the measurements. Further we acknowledge DST, India for providing facility for the SQUID and FTIR measurements at Indian Institute of Science, Bangalore. Finally we acknowledge S.S.P.L., Delhi, India for providing CdZnTe samples.

References

[1] C.K. Ard, in: P. Capper (Ed.), Properties of Narrow Gap Cadmium Based Compounds, INSPEC, IEE Publishing, London, 1994, pp. 598–603.
[2] P. Capper, M.G. Astles, D.J. Williams, P. Mackett, P. Franzosi, S. Bernardi, L. Svob, in: P. Capper (Ed.), Properties of Narrow Gap Cadmium Based Compounds, INSPEC, IEE Publishing, London, 1994, pp. 487–534.
[3] A.K. Garg, M. Srivastava, R.C. Narula, R.K. Bagai, V. Kumar, J. Cryst. Growth 260 (2004) 148–158.
[4] S. Sitharaman, R. Raman, L. Durai, S. Pal, M. Gautam, A. Nagpal, S. Kumar, S.N. Chatterjee, S.C. Gupta, J. Cryst. Growth 285 (2005) 318–326.
[5] G.A. Kulkarni, V.G. Sathe, K.S.R.K. Rao, D.V.S. Muthu, R.K. Sharma, J. Appl. Phys. 105 (2009) 063512-1–063512-6 and the references there in.
[6] B.M. Vul, V.S. Ivanov, V.A. Rukavishnikov, V.M. Sal'man, V.A. Chapnin, Sov. Phys. Semiconduct. 6 (1973) 1106–1109.
[7] G.A. Slack, S. Galginaitis, Phys. Rev. 133 (1964) A253–A268.
[8] P. Capper, J. Cryst. Growth 57 (1982) 280–299.
[9] S.A. Wolf, D.D. Awschalom, R.A. Buhrman, J.M. Daughton, S. von Molnar, M.L. Roukes, A.Y. Chtchelkanova, D.M. Treger, Science 294 (2001) 1488–1495.
[10] D.R. Sharma, B.R. Chakraborty, M.L. Das, Appl. Surf. Sci. 135 (1998) 193–199.
[11] H. Watanabe, J. Phys. Chem. Solids 25 (1964) 1471–1475 and the references there in.
[12] I. Fidone, K.W.H. Stevens, Proc. Phys. Soc. London 73 (1959) 116–117.
[13] D. Saurel, A. Brulet, A. Heinemann, C. Martin, S. Mercone, C. Simon, Phys. Rev. B 73 (2006) 094438-1–094438-9.
[14] F.J. Dyson, Phys. Rev. 98 (1955) 349–359.
[15] G. Feher, A.F. Kip, Phys. Rev. 98 (1955) 337–348.
[16] J.P. Joshi, S.V. Bhat, J. Magn. Reson. 168 (2004) 284–287.
[17] R.C. Bowman Jr., D.E. Cooper, Appl. Phys. Lett. 53 (1988) 1521–1523.
[18] V.N. Smolyaninova, J.J. Hamilton, R.L. Greene, Y.M. Mukovskii, S.G. Karabashev, A.M. Balbashov, Phys. Rev. B 55 (1997) 5640–5642.
[19] G.A. Slack, S. Roberts, J.T. Vallin, Phys. Rev. 187 (1969) 511–524.
[20] E.E. Vogel, J.R. Iratchet, Phys. Rev. B 22 (1980) 4511–4522.
[21] P. Emanuelsson, P. Omling, B.K. Meyer, M. Wienecke, M. Schenk, Phys. Rev. B 47 (1993) 15578–15581.